Timing of charge migration in betaine by impact of fast atomic ions

Patrick Rousseau, Jesús González-Vázquez, Dariusz G Piekarski, Janina Kopyra, Alicja Domaracka, Manuel Alcamí, Lamri Adoui, Bernd A Huber, Sergio Díaz-Tendero, Fernando Martín

Timing of charge migration in betaine by impact of fast atomic ions

P. Rousseau,[1*] J. González-Vázquez[2,3*], D.G. Piekarski,[2,○] J. Kopyra,[4]
A. Domaracka[1], M. Alcamí,[2,3,5] L. Adoui,[1] B. A. Huber,[1]
S. Díaz-Tendero,[2,3,6,†] F. Martín[2,5,6,‡]

[1]Normandie Univ, ENSICAEN, UNICAEN, CEA, CNRS, CIMAP, 14000 Caen, France.
[2]Departamento de Química, Módulo 13, Universidad Autónoma de Madrid, 28049 Madrid, Spain.
[3]Institute for Advanced Research in Chemical Sciences (IAdChem), Universidad Autónoma de Madrid, 28049 Madrid, Spain.
[4]Faculty of Exact and Natural Sciences, Siedlce University of Natural Sciences and Humanities, 3 Maja 54, 08-110 Siedlce, Poland.
[5]Instituto Madrileño de Estudios Avanzados en Nanociencias (IMDEA Nano), Cantoblanco 28049 Madrid, Spain
[6]Condensed Matter Physics Center (IFIMAC), Universidad Autónoma de Madrid, 28049 Madrid, Spain.

[*]These authors contributed equally

[○]Present address: Institute of Physical Chemistry, Polish Academy of Sciences, Kasprzaka 44/52, 01-224 Warsaw, Poland.

[†]sergio.diaztendero@uam.es
[‡]fernando.martin@uam.es

The way molecules break after ion bombardment is intimately related to the early electron dynamics generated in the system, in particular, charge (or electron) migration. We exploit the natural positive-negative charge splitting in the zwitterionic molecule betaine to selectively induce double electron removal from its negatively charged side by impact of fast O^{6+} ions. The loss of the two electrons in such a localized region of the molecular skeleton triggers a competition between direct Coulomb explosion and charge migration that is examined to obtain temporal information from ion-ion coincident measurements and non-adiabatic molecular dynamics calculations. We find a charge migration time, from one end of the molecule to the other, of approximately 20-40 fs. This migration time is longer than that observed in molecules irradiated by ultrashort light pulses and is the consequence of charge migration being driven by adiabatic nuclear dynamics in the ground state of the molecular dication.

Teaser

Timing adiabatic charge migration in doubly charged betaine ions resulting from collisions with highly charged ions

Introduction

Understanding and controlling molecular damage induced by ionizing radiation, such as extreme-ultraviolet (XUV) or X-ray light, fast electrons or ions, is one of the current challenges in natural sciences. Indeed, it is well established that molecular damage can lead, among other processes, to random mutagenic miscoding or even lethal nanocoding of the DNA sequence, which is at the origin of several diseases (*1–4*). However, when conveniently controlled, ionizing ir-radiation can be the remedy rather than the problem, as demonstrated by current radio- and hadron-therapies (*5, 6*). An important source of damage is the environment surrounding the molecule and, in this respect, several processes involving electron transfer between neighboring molecules have been proposed, as electron-transfer-mediated decay (ETMD) (*7*) or interatomic Coulombic decay (ICD) (*8*). However, pioneering experimental and theoretical work (*9, 10*) has shown not only that molecular damage is also possible in isolated molecules, but also that the nature of the resulting fragments is intimately related to the charge migration induced by the ionizing radiation at the very early stages, where most of the dynamics is governed by electronic motion. To experimentally investigate these early stages, one must first access the natural time scale of electronic motion, i.e., from several hundreds attoseconds to a few femtoseconds, and then follow the ensuing coupled electron and nuclear dynamics within the next few tens of femtoseconds.

This is nowadays possible by using XUV/X-ray attosecond and few fs pulses produced either in the laboratory through high harmonic generation (HHG) or in large-scale X-ray free-electron laser (FEL) facilities, usually in the framework of pump-probe set ups (*11–16*). The necessary time resolution is achieved by using a short enough pump pulse, so that ionization is a ”sudden” process in comparison with the subsequent charge migration process, which can then be probed by using a second ultrashort pulse and varying the pump-probe delay with attosecond

and few-fs resolution. In these experiments, charge migration results from the coherent superposition of electronic states created by the broadband pump pulse in the remaining molecular cation and, therefore, it precedes nuclear motion (*13, 16*) -although nuclear motion can have a significant effect at longer times (*17, 18*). In the case of X-ray pulses, the sudden ionization of the molecule can be followed by Auger decay, which can thus induce charge migration in the corresponding molecular dication (*17, 19*). One can also use ultrafast molecular dissociation associated to, e.g., proton emission or Coulomb explosion or both, to clock the electron dynamics generated by the pump pulse. With the help of accurate theoretical calculations (see, e.g., (*16, 20, 21*) and references therein), the latter methods have been able to provide real-time pictures of electron dynamics in small and medium-size molecules ionized by IR, XUV and X-ray light (*22–26*).

Charge migration induced by fast ions and electrons is, in general, very different from that induced by photons, as the latter usually involve less electronic channels as a result of selection rules. Also, contrary to photons (and electrons), ions can selectively deposit energy in a well localized region of a bulky target, as they can efficiently penetrate matter with low rates of diffusion and release most of their energy all at once just before stopping (the so called Bragg peak) (*27–29*). So they are ideal, e.g., to treat tumors where extreme spatial localization is essential. Hence, understanding charge migration induced in collisions with atomic ions is not only important per se but also to explore new routes to trigger radiation damage by altering the early electron dynamics.

Such studies require the implementation of specific experimental and theoretical approaches. In recent pump-probe experiments, ultrashort femtosecond pulses of electrons pioneered by Zewail and collaborators (*30*) have been successfully combined with ultrashort laser pulses with a time resolution of $\sim$150 fs (*31*), which is comparable to that achieved in state-of-the-art femtochemistry experiments performed with lasers but provide in addition spatial atomic resolution.

In the case of atomic ions, this is not yet possible, mainly due to the difficulty to produce ultrashort pulsed ionic beams in conventional ion accelerators. And this in spite of the fact that an ion of approximately a few keV/amu interacts with a small or medium size molecule for no more than a few fs (e.g., a 3 keV/amu projectile has a velocity of 7.6 Å/fs), which is the optimum scenario to induce a "sudden" ionization of the molecular target, hence to investigate charge migration processes in their natural time scale. To achieve the necessary few-fs time resolution, in this work, we will use ultrafast Coulomb explosion as an internal clock of the electron dynamics generated by the ionizing collision. This is not always an available option, but, as we will see below, it can be achieved by a smart selection of the ionic projectile and molecular target.

Here, we exploit the natural positive-negative charge splitting in the betaine zwitterion ($N, N, N-$trimethylglycine, see Fig. 1c) to selectively induce double ionization on the negatively charged end of the molecule by impact of 3 keV/amu O^{6+} and then trigger a competition between direct Coulomb explosion and charge migration involving the two positively charged ends of the doubly ionized molecule. The analysis of the kinetic energy distributions of the resulting positively charged fragments detected in coincidence along with the results of ab initio non-adiabatic molecular dynamics simulations allows us to determine a charge migration time from end to end of approximately 20-40 fs. The calculations also show that charge migration is mainly driven by nuclear motion in the ground state of the molecular dication, thus leading to migration times longer than those observed in charge migration triggered by electronic coherences (*13, 16, 32*).

Results and discussion

With a positive charge localized on the quaternary ammonium group ($-\mathrm{N}^{+}(\mathrm{CH}_3)_3$) and a negative charge on the carboxylate group ($-\mathrm{CO}_2^{-}$) (see Fig. 1c), the (neutral) betaine molecule

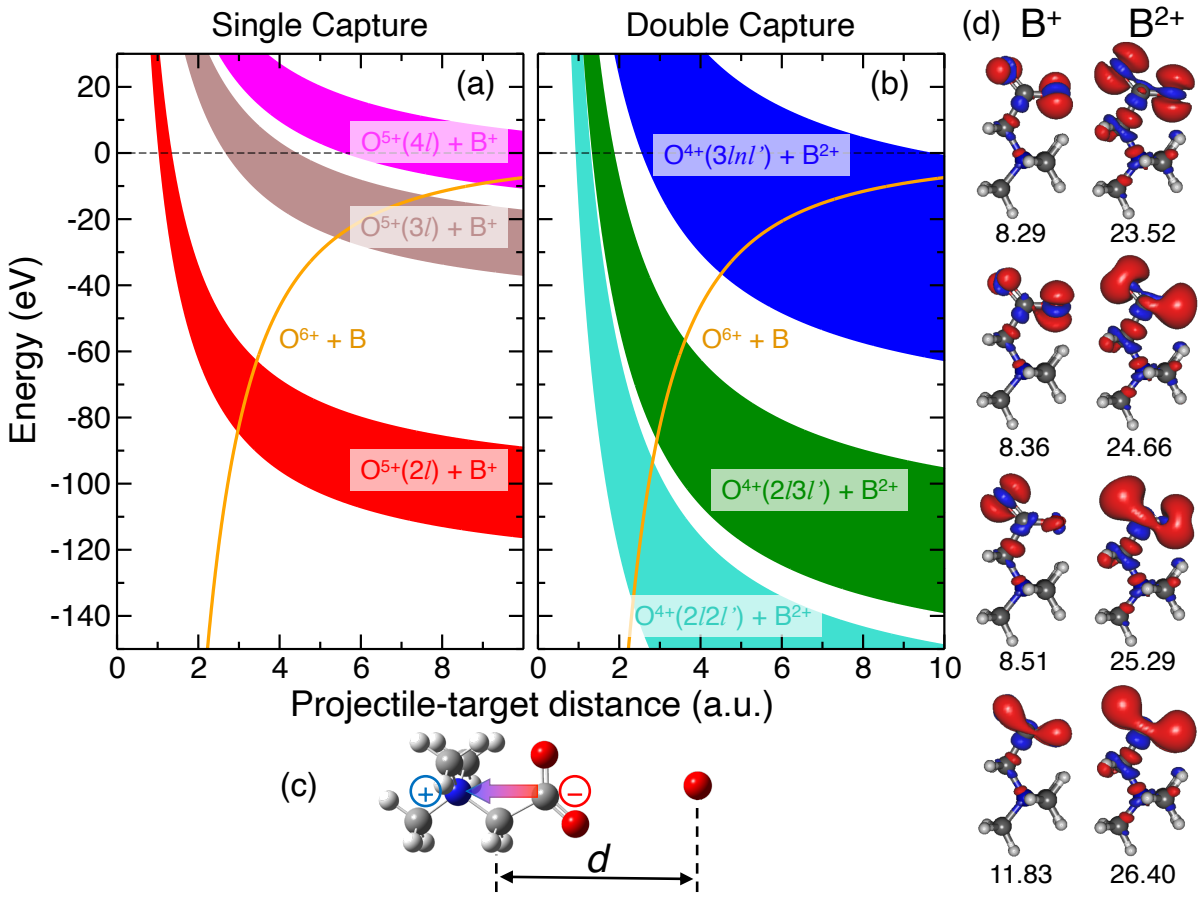

Figure 1: **The O^{6+} – betaine system.** Molecular energies for (a) single-electron capture and (b) double-electron capture channels as a function of the distance between the O^{6+} projectile and the center of mass of the betaine molecule oriented as shown in panel (c). For the sake of clarity, only the energy ranges covered by the single- and double-electron capture channels leading to $O^{5+}(nl)$ with $n < 5$ (a) and $O^{4+}(2lnl')$ with $n < 4$ and $O^{4+}(3lnl')$ (b) are shown. The missing channels are expected to be barely populated in the collision or lie outside the axes range. Notice that the incoming projectile approaches the molecule from the side of the negatively charged carboxylate group, which is the most favorable orientation for single and double capture (see text). The orange curves in (a) and (b) represent the entrance channel. The electron densities, referred to the ground state electron density of neutral betaine, for the lowest states of singly- and doubly-charged betaine resulting from single- and double-electron capture, respectively, are shown in panel (d). The numbers below the density maps indicate the energies (in eV) of the corresponding electronic states of singly- and doubly-charge betaine with respect to the energy of the ground state of neutral betaine.

($N(CH_3)_3 - CH_2 - COO$) has a rather large permanent dipole of 11.5 Debyes (4.5 a.u.) (*33*). Figures 1a,b show the potential energy curves of the $[O^{6+}-B]$ system (where B stands for betaine) for the case in which the O^{6+} projectile lies in the direction of the betaine permanent dipole μ (Fig. 1c). The orientation of the molecule is such that the charge-dipole interaction between the projectile (P) and the target (T) is the most attractive. The potential energy curves and the energy ranges associated with the single- and double-capture channels have been obtained by using the experimental bound-state energies of O^{6+}, O^{5+} and O^{4+} (*34*), the calculated energies of the autoionizing doubly-excited states of O^{4+} (*35*), the calculated first, second and third vertical ionization potentials of betaine (see Methods for details), and the asymptotic analytical formulas that describe the repulsive charge-charge, $q_P q_T/d$, and attractive charge-dipole, $q_P(\boldsymbol{\mu}\cdot\mathbf{d})/d^3$, interactions between the different projectile and target species, where d is the distance between the projectile and the center of mass of the target (*36*). The latter formulas are expected to accurately represent the actual behavior of the potential energy curves except at very short projectile-target distances, where electron delocalization over the projectile and the target can be important. As can be seen, the potential energy curve of the entrance channel $O^{6+}-B$ intersects the repulsive curves of the $O^{4+}(1s^2 3l n l')-B^{2+}$ channels, associated with double electron capture, at projectile-target distances between 5 a.u. and $\sim$10 a.u., where non adiabatic transitions from the former to the latter channels should be very efficient at the impact energy considered in this work (*37*). The same applies to the $O^{5+}(1s^2 3l)-B^{+}$ and $O^{5+}(1s^2 4l)-B^{+}$ channels, associated with simple capture, which appear in the same energy region as the double-capture channels. Therefore, one can expect that both single and double electron capture (either direct or mediated by single-capture channels) will be very efficient processes. These are also expected to occur, though to a lesser extent, when the molecule is oriented at 90^o with respect to the incidence direction, as $\boldsymbol{\mu}\cdot\mathbf{d} = 0$ and the corresponding potential energy curve mostly coincides with the zero-energy axis. This curve crosses single- and double-electron capture

channels in a similar range of projectile-target distances, although involving slightly higher n and l quantum numbers in the projectile side, which are less favorable due to the large number of radial and angular nodes in the corresponding wave functions (Barat-Lichten rules (*38*)). More importantly, if the orientation of the betaine molecule was reversed with respect to the first one, the potential energy curve of the entrance channel would be the mirror image of that shown in Figs. 1a,b with respect to the zero-energy axis, i.e., it would be entirely repulsive and therefore would not lead to significant single and double capture in the above mentioned channels. In other words, the charge-dipole interaction that governs the approach of the projectile to the target and the orientation selectivity of the double-capture process restrict the range of molecular orientations where doubly charged betaine can be formed. We can safely discard ionization as a possible source of doubly charged betaine because, for the impact energy considered in our work (3 keV/amu), the ionization cross section is several orders of magnitude smaller than that associated with electron capture (see, e.g., references (*39, 40*) for the case of proton-hydrogen and proton-uracil collisions). For the same reason, transfer-ionization and electron-transfer-mediated decay (ETMD) (*7, 41*), in which a betaine electron directly goes into the continuum (ionization) and another betaine electron is transferred to the projectile (capture) thus leading to a betaine dication, are expected to be less likely than two resonant electron transfers to the projectile (*39, 40, 42*). Finally, two-electron processes implying the removal of electrons from inner shells (non resonant electron capture) can also be discarded because target inner vacancy states lie very far in energy from the entrance channel (in fact, these states lie out of scale in Fig. 1).

Figure 1d shows the electron density of the four lowest states of singly- and doubly-ionized betaine referred to the ground sCMtate density of neutral betaine. As can be seen, the removal of one or two electrons always involves the $-CO_2^-$ side of the zwitterion, meaning that, after double capture (either direct or sequential), this side of the molecule will hold a positive charge

while the charge distribution in the rest of the molecule will basically remain unchanged. This fact, combined with the high preference for the molecular orientation shown in Fig. 1c, indicates a high selectivity of the double electron capture process, which basically leads to a doubly charged betaine molecule with a positively charged $-CO_2^+$ side and a positively charged $-N(CH_3)_3^+$ side, well separated from each other. These are the optimal conditions for a clean and rapid Coulomb explosion (CE) of B^{2+}, which is expected to compete with internal charge migration (CM), where an electron would move from the $-N(CH_3)_3^+$ side to the $-CO_2^+$ high electron-affinity side, thus neutralizing the positive charge in the latter side. The two competing processes are expected to lead to different molecular fragments, as illustrated in Figure 2a: CE can lead to CO_2^+ and other molecular fragments, while CM is not expected to lead to any CO_2^+.

In order to confirm this picture, we have performed ion-ion coincident measurements of the ionic fragments produced in collisions of 3 keV/amu O^{6+} with fully deuterated betaine. We have chosen deuterated betaine in order to unambiguously assign fragments using time-of-flight mass spectrometry (e.g., both $N(CH_3)_2^+$ and CO_2^+ have $m/z = 44$ while $N(CD_3)_2^+$ has $m/z = 50$). Figures 2b,c show zooms in regions of the ion-ion coincidence map around the $(m_1/z_1)^+/(m_2/z_2)^+$ islands $18^+/66^+$ and $44^+/66^+$, corresponding to, respectively, $CD_3^+/(CD_2)N(CD_3)_2^+$ and $CO_2^+/(CD_2)N(CD_3)_2^+$ coincidences. The full ion-pair coincidence map is given in the Supplementary Material. The $44^+/66^+$ island arises from direct CE of doubly charged betaine into $CO_2^+/(CD_2)N(CD_3)_3^+$ and the subsequent emission of a neutral methyl group (CD_3) from the larger fragment, thus leading to $CO_2^+/(CD_2)N(CD_3)_2^+/CD_3$. This two-step mechanism is confirmed by the slope of the $44^+/66^+$ island, which is approximately $-66/(66+18)$, suggesting also that the neutral CD_3 fragment emitted in the second step has a negligible momentum (see Refs. (*43, 44*) for the connection between the slopes of coincident islands and n-body fragmentation).

The $18^+/66^+$ island is associated with three body fragmentation of doubly charged betaine

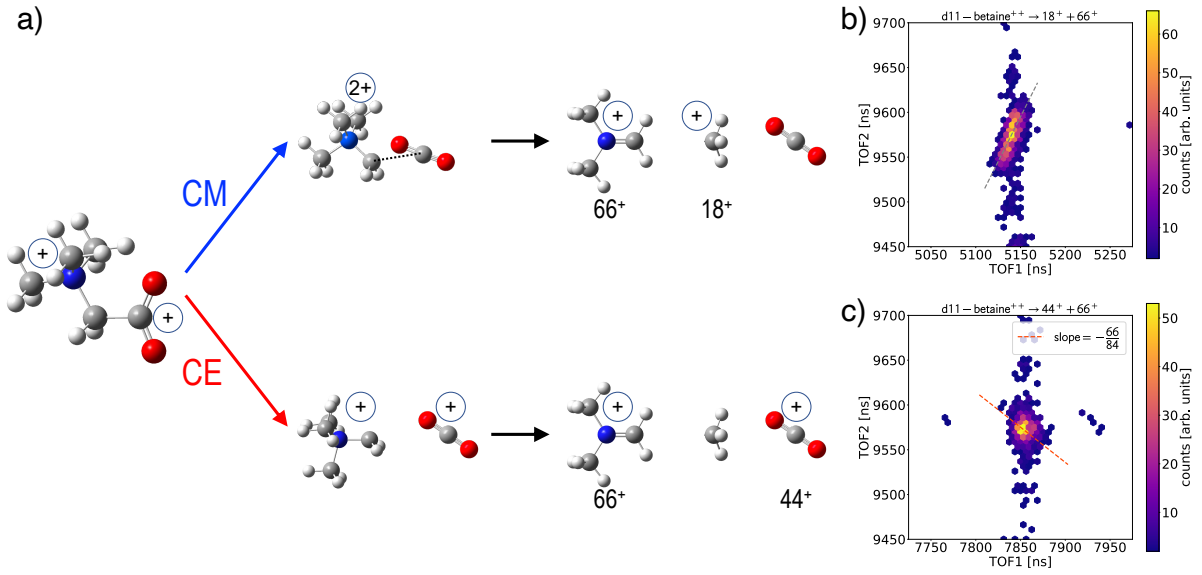

Figure 2: **Fragmentation of fully deuterated doubly charged betaine.** (a) As a result of double electron capture by the projectile from the carboxylate group, both ends of the betaine molecule are positively charged. Two scenarios are then possible: direct Coulomb explosion (CE) and charge migration (CM). In CE, charge separation by cleavage of the $C_{carboxylate}-C_{\alpha}$ bond leads to the two charged fragments $CCMO_2^+$ and $(CD_2)N(CD_3)_3^+$. The latter further dissociates by emission of a neutral methyl group CD_3. Experimentally, this process leads to a coincidence $44^+/66^+$ in the ion-ion map (c). The slope of the measured island, given by momentum conservation, confirms this scheme (see text). In contrast, after CM, the ammonium side of the betaine is doubly charged, so that the emission of a neutral carboxylate group CO_2 is expected and the ulterior charge separation gives rise to two charged fragments, CD_3^+ and $(CD_2)N(CD_3)_2^+$. Experimentally, one observes a coincidence island $18^+/66^+$ in the ion-ion map (b) with a positive slope, indicating that fragmentation involves the formation of the intermediate species shown in the upper row of (a) (see text).

after neutralization of the $-CO_2$ side by CM, leading to $CO_2/CD_3^+/(CD_2)N(CD_3)_2^+$. In this case, the slope of the coincidence island is positive and cannot be explained as resulting from a two-step process in which Coulomb explosion is followed by emission with negligible momentum of neutral CO_2 from one of the charged fragments, as this process would always lead to an island with negative slope. A positive slope indicates that the two charged fragments are emitted in the same direction (*45*), while neutral CO_2 is emitted with large momentum in the opposite direction to compensate the momentum of the charged particles. This picture is consistent with the formation of an intermediate doubly-charged transient structure as that shown in the upper panel of Fig. 2a, which, according to our calculations (see below), corresponds to a minimum in the potential energy surface arising from the attractive charge / induced-dipole interaction between $(CD_2)N(CD_3)_3^+$ and a neutral CO_2 fragment in the early stages of dissociation.

To get a deeper insight on the results of these measurements, we have performed few-switches trajectory surface hopping (FS-TSH) calculations on the lowest potential energy surfaces of the betaine dication obtained within the complete active space perturbation theory (CASPT2) approach (see Methods for details). Figure 3 summarizes the most important results. Panel (a) shows the time evolution of the local charge around the CO_2 group for trajectories starting from the ground and first excited state of the betaine dication. As can be seen, within the limited time interval considered in our calculations (see Supplementary Material for an extension up to 150 fs), trajectories starting in the ground state can only lead to CO_2 charges equal to zero or around +0.75, which are consistent with the charges that should be observed just after CM or in the intact betaine dication, respectively. In contrast, trajectories starting in the first excited state can only lead to CO_2 charges equal to +1 or around +0.75, compatible with CE and the intact betaine dication, respectively. Trajectories starting in the second excited state (not shown in the figure for the sake of clarity, see Supplementary Material) follow a similar pattern: they do not lead to neutral CO_2. Panel (a) also shows that neutralization of the initial positive

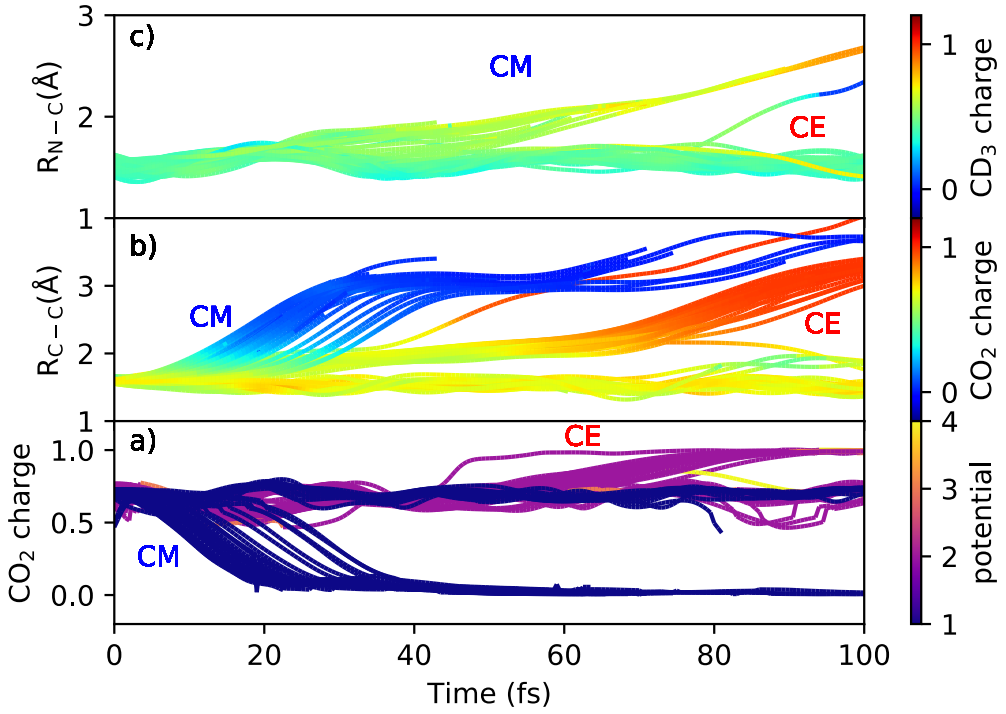

Figure 3: **Molecular dynamics calculations.** (a) Evolution of the charge located at the CO_2 end of doubly-charged betaine for all trajectories starting in the ground (1) and the first excited (2) state. The color palette on the right indicates the potential energy surface in which the trajectory evolves at every time. Notice that a significant number of trajectories starting in the ground state lead to neutralization of the CO_2 end. (b) Evolution of the $C_{\mathrm{carboxylate}}-C_\alpha$ bond distance in doubly-charged betaine for all trajectories starting in the ground and the first excited state. The color palette on the right indicates the charge in the CO_2 end at every time. Notice that the $C_{\mathrm{carboxylate}}-C_\alpha$ bond breaks faster in CM than in CE. (c) Evolution of the N−C bond distance in doubly-charged betaine for all trajectories starting in the ground and the first excited state. The color palette on the right indicates the charge in the CD_3 site at every time.

charge in the CO_2 site is completed in 20 to 40 fs, while acquiring the +1 charge required for CE takes around 100 fs.

Panels (b) and (c) show that the times needed by CO_2 to acquire its final charge strongly correlate with the times needed by the charged molecular fragments to complete the dissociation process. Indeed, as can be seen in panel (b), when CO_2 becomes completely neutral after 20-40 fs, the C-C distance has increased by more than 1 Å (i.e., more than 2 a.u.), while it remains almost unchanged for those trajectories leading to a charge +1 in the CO_2 side. In the latter case, a variation of 1 Å in the C-C distance is only observed after approximately 100 fs, showing that acquiring the right +1 charge and fragmenting are concerted processes. CD_3^+ fragments associated with CM acquire their final +1 charge in about 100 fs (see panel (c)), while in the case of CE, the CD_3 sites preserve their initial charge at all times. Interestingly, the C-C distance remains more or less constant for around 20 fs after neutralization of the CO_2 end (panel (b)) but, with no exception, emission of neutral CO_2 is irreversibly produced at later times. The existence of such a plateau in the C-C distance is due to the transient formation of the doubly-charged complex depicted in Fig. 2a, which delays for about 20 fs the ejection of neutral CO_2 and the ensuing fragmentation of the remaining dication into $CD_3^+/(CD_2)N(CD_3)_2^+$. This result is compatible with the observation of a positive slope in the $18^+/66^+$ island, since the fact that CO_2 leaves first makes the two charged fragments go in the same direction (i.e., opposite to the CO_2 emission direction).

The results given in Fig. 3 show that CM is mostly an adiabatic process taking place in the ground state of the betaine dication. This interpretation is confirmed by the absence of avoided crossings between the ground and the excited electronic states of doubly charged betaine and the conservation of the ground-state electronic character along the minimum energy path leading to emission of neutral CO_2 (see Supplementary Information). So, CM is almost entirely driven by nuclear motion in this ground state, which explains why CM in doubly-charged betaine is

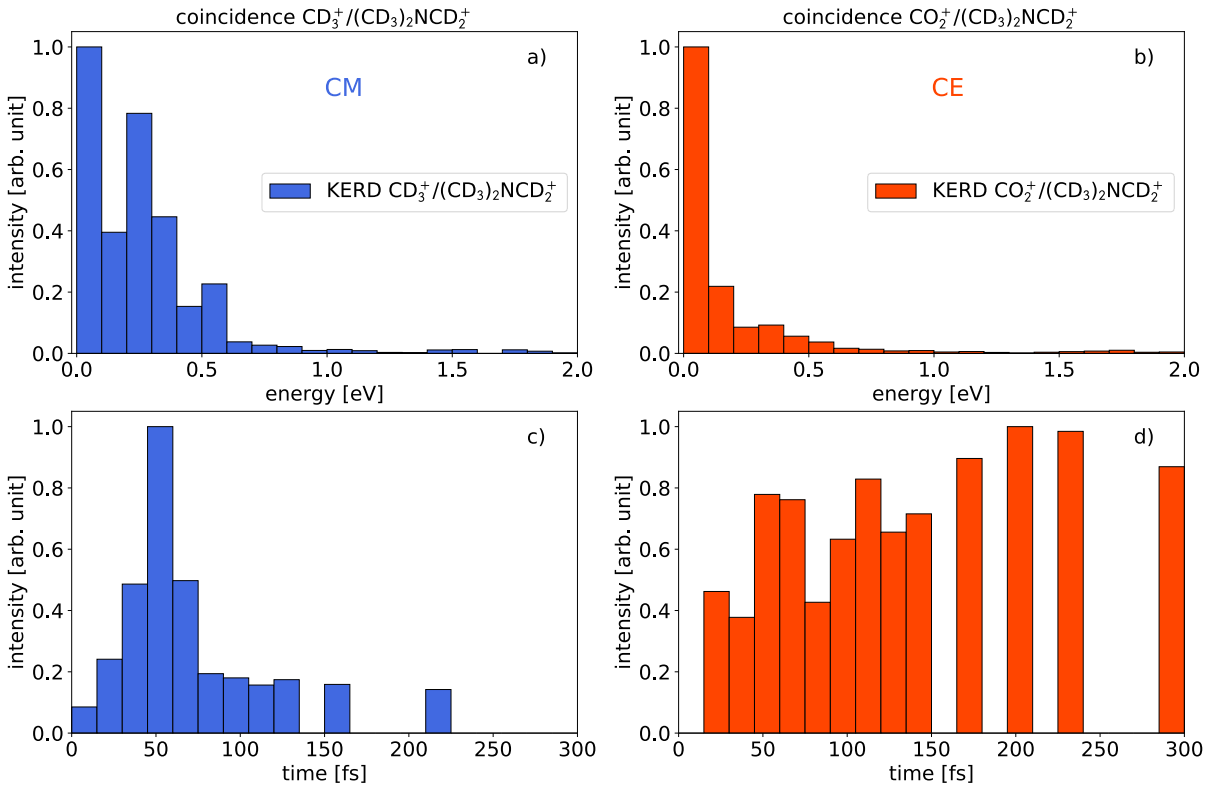

Figure 4: **Kinetic energy release and estimation of the charge separation time.** Kinetic energy release (KER) for (a) CD_3^+ fragments detected in coincidence with 66^+ fragments (associated with CM), and (b) CO_2^+ fragments detected in coincidence with 66^+ fragments (associated with direct CE). (c) and (d) Estimation of the time necessary for the separation of the two charges leading to the corresponding ion pairs $18^+/66^+$ and $44^+/66^+$ based on their respective kinetic energy release distribution.

substantially slower than charge fluctuations resulting exclusively from electronic coherences induced by ionizing radiation, e.g., by using attosecond and few-fs laser or electron pulses.

An analysis of the kinetic energy release (KER) of the $CD_3^+/(CD_2)N(CD_3)_2^+$ and $CO_2^+/(CD_2)N(CD_3)_2^+$ ion pairs associated with, respectively, the $18^+/66^+$ and $44^+/66^+$ peaks observed in the ion-ion coincidence spectrum confirms the general trends resulting from our calculations. The details of this analysis are given in the Methods section and the Supplementary Information. The KERs are shown in Figs. 4a,b, respectively, in the form of histograms.

Both distributions peak at zero kinetic energy and decrease with energy. However, the KER associated with CE (i.e., the CO_2^+ /$(CD_2)N(CD_3)_2^+$ coincidence) is significantly narrower, indicating that CE (or, equivalently, emission of CO_2^+) is slower than the fragmentation into CD_3^+/$(CD_2)N(CD_3)_2^+$ that follows CM (see Fig. 2a). This fact can be more clearly seen in Figs. 4c,d, where the corresponding kinetic energy release (KER) histograms have been converted into time histograms by assuming that direct CE and CD_3^+ emission following CM are practically irreversible when the two charged fragments have travelled a distance of 2 a.u. from their initial positions. As can be seen, for CM, the time histogram peaks at around 50 fs, whereas, for CE, approximately 90% of the events take much longer than 50 fs, in excellent agreement with our theoretical findings, in particular with our estimation of the CM time. Interestingly, the time histogram for direct CE given in Fig. 4d shows an increase of the number of events at around 50 fs, which is more or less the time taken by CM to occur. When direct CE is that fast, one can expect that it efficiently competes with CM, thus highlighting the effect of possible electronic coherences between the CE and CM channels. Since determination of the kinetic energy of the fragments from the measured TOF distribution is not as accurate as that provided by position sensitive detectors, further experimental work allowing for the direct measurement of fragments momentum could shed more light on this issue and probably allow for a more accurate retrieval of the CM time from experiment by focusing on the KER region where interferences between CE and CM channels are expected to occur.

Conclusion

Taking advantage of the natural positive-negative charge separation in the betaine zwitterion, we have been able to selectively induce double electron removal from the negatively charged end of the molecule in collisions with 3 keV/amu O^{6+} ions. This process initiates a competition between direct Coulomb explosion and charge migration that can be used to obtain temporal

information on the several stages involved in these processes. We have determined an internal charge migration time, from one end of the molecule to the other, of approximately 20-40 fs and show that this process preferentially takes place in the ground state of the betaine dication resulting from the collision, while direct Coulomb explosion mainly occurs in its excited states. The charge migration time is significantly longer than that previously observed in charge dynamics induced by electronic coherences in molecules of similar complexity. This is the consequence of charge migration being mostly driven by adiabatic nuclear dynamics in the ground state of the betaine dication.

Methods

Experiment

The experiments have been performed at ARIBE (*46*), the low-energy ion beam facility of GANIL (Caen, France). The experimental set-up and methods have been described in detail elsewhere (*47*). Briefly, the O^{6+} ions are produced in an electron cyclotron resonance ion source, accelerated at 48 keV and mass-analyzed by a magnet sector. The beam is pulsed in bunches of 500 ns and transported by ion optics towards the crossed-beam collision device where after focusing it interacts with an effusive beam of neutral betaine molecules produced by evaporation of a commercial sample of fully deuterated betaine (purity 98%, Eurisotop) in a heated oven. Just after the passage of the ion bunch, the cationic products of the interaction are extracted by a pulsed electric field into a modified Wiley-McLaren time-of-flight mass spectrometer (*48*). Their arrival times are recorded in an event-by-event mode allowing to consider coincidences among them (*49, 50*). The kinetic energy release of an ion pair is obtained after differentiation of the distribution of the time difference between two fragments (*51, 52*). SIMION simulations of the time-of-flight spectrometer show that the ion transmission is 100% for cations with a kinetic energy up to 10 eV (*53*). From the relative velocity of the two frag-

ments one can estimate the time required to run a given distance.

Theory

Optimized geometry and frequencies for the betaine molecule were obtained in the ground electronic state using the Moller-Plesset (MP2) method with the cc-pvDZ-jkfit basis (*54*) as implemented in the BAGEL code (*55*). Starting from this geometry, a set of 50 initial conditions were obtained using a harmonic Wigner distribution of correlated position and momentum. In order to describe the electronic states of the different ionization states of betaine, single point state-average complete active space self-consistent field (SA-CASSCF) calculations were performed for the neutral (singlet), cation (doublet), dication (singlet and triplet) and trication (doublet) at the MP2 geometry using a state average of 4 electronic states, without symmetry considerations, with an active space consisting of 8 orbitals and 8 electrons for the neutral species. These calculations were performed by using the OpenMOLCAS package (*56*) with the same basis set. To simulate the non-adiabatic semiclassical dynamics, a local version of the SHARC (*57*) method was employed. The electronic structure was represented, including gradients, at the XMS-CASPT2 level (*58*) with an imaginary shift of 0.2 a.u. by using the BAGEL code (*55*). For the calculation of the non-adiabatic couplings, the overlap matrix between two consecutive time steps was employed. For this, the perturbed modified wave function, including configuration interaction (CI) vectors and molecular orbitals, was extracted from BAGEL (*55*) and imported into the OpenMOLCAS code (*56*) with overlaps obtained with the RASSI program. Charges on different molecular sites were evaluated by performing a Mulliken analysis.

Acknowledgments

All calculations were performed at the Mare Nostrum Supercomputer of the Red Española de Supercomputación (BSC-RES) and the Centro de Computación Científica de la Universi-

dad Autónoma de Madrid (CCC-UAM). Work supported by the MICINN projects PID2019-105458RB-I00, PID2019-106732GB-I00 and PID2019-110091GB-I00, the "Severo Ochoa" Programme for Centres of Excellence in R&D (SEV-2016-0686), the "María de Maeztu" Programme for Units of Excellence in R&D (CEX2018-000805-M), and the European COST Actions CA18212 MD-GAS and CA18222 AttoChem. The research was conducted in the framework of the International Associated Laboratory (LIA - CNRS) "Fragmentation DYNAmics of complex MOlecular systems - DYNAMO". J.K. acknowledges support for a visit to GANIL, Caen (France) from the Polish Ministry of Science and Higher Education via statutory activity subsidy (No 25/20/B).

Data and Materials Availability

All data needed to evaluate the conclusions in the paper are present in the paper and/or the Supplementary Materials.

Author Contributions

PR, JK, AD and BH designed and performed the experiments and analyzed the experimental data. JGV, DGP, SDT and FM designed and performed the theoretical calculations and analyzed the theoretical data. All authors discussed the results. PR, SDT and FM wrote the first version of the manuscript and all authors contributed to their improvement. FM coordinated the project.

Competing Interests

The authors declare no competing interests.

References

1. B. Boudaïffa, P. Cloutier, D. Hunting, M. A. Huels, L. Sanche, *Science* **287**, 1658 (2000).

2. C. E. Crespo-Hernández, B. Cohen, P. M. Hare, B. Kohler, *Chemical Reviews* **104**, 1977 (2004).

3. *DNA Damage Recognition* (Taylor & Francis, New York, 2006), W. Siede and Y. W. Kowband and P. W. Doetsch edn.

4. R. P. Sinha, D.-P. Hder, *Photochem. Photobiol. Sci.* **1**, 225 (2002).

5. *Principles of Radiation Oncology in Cancer* (Lippincott Williams and Wilkins, Philadelphia, 2008), V. T. DeVita Jr. and T. S. Lawrence and S. A. Rosenberg edn.

6. M. Durante, J. S. Loeffler, *Nat. Rev. Clin. Oncol.* **7**, 37 (2010).

7. V. Stumpf, K. Gokhberg, L. S. Cederbaum, *Nature Chemistry* **8**, 237 (2016).

8. L. S. Cederbaum, J. Zobeley, F. Tarantelli, *Phys. Rev. Lett.* **79**, 4778 (1997).

9. R. Weinkauf, P. Schanen, D. Yang, S. Soukara, E. W. Schlag, *The Journal of Physical Chemistry* **99**, 11255 (1995).

10. R. Weinkauf, E. W. Schlag, T. J. Martinez, R. D. Levine, *The Journal of Physical Chemistry A* **101**, 7702 (1997).

11. G. Sansone, *et al.*, *Nature* **465**, 763 (2010).

12. L. Belshaw, *et al.*, *The Journal of Physical Chemistry Letters* **3**, 3751 (2012).

13. F. Calegari, *et al.*, *Science* **346**, 336 (2014).

14. P. Ranitovic, *et al.*, *Proceedings of the National Academy of Sciences* **111**, 912 (2014).

15. A. Marciniak, *et al.*, *Nat. Commun.* **10**, 337 (2019).

16. M. Nisoli, P. Decleva, F. Calegari, A. Palacios, F. Martín, *Chemical Reviews* **117**, 10760 (2017).

17. C. Arnold, O. Vendrell, R. Santra, *Phys. Rev. A* **95**, 033425 (2017).

18. J. Delgado, *et al.*, *Faraday Discuss.* pp. – (2021).

19. A. Picón, C. Bostedt, C. Hernández-García, L. Plaja, *Phys. Rev. A* **98**, 043433 (2018).

20. A. I. Kuleff, L. S. Cederbaum, *Journal of Physics B: Atomic, Molecular and Optical Physics* **47**, 124002 (2014).

21. M. Kowalewski, B. P. Fingerhut, K. E. Dorfman, K. Bennett, S. Mukamel, *Chemical Reviews* **117**, 12165 (2017). PMID: 28949133.

22. M. Pitzer, *et al.*, *Science* **341**, 1096 (2013).

23. A. Rudenko, *et al.*, *Nature* **546**, 129 (2017).

24. T. Yatsuhashi, N. Nakashima, *Journal of Photochemistry and Photobiology C: Photochemistry Reviews* **34**, 52 (2018).

25. F. Allum, *et al.*, *The Journal of Chemical Physics* **149**, 204313 (2018).

26. R. Y. Bello, *et al.*, *Sci. Adv.* **4**, aat3962 (2018).

27. U. Amaldi, G. Kraft, *Reports on Progress in Physics* **68**, 1861 (2005).

28. D. Kramer, *Physics Today* **68**, 24 (2015).

29. D. Schulz-Ertner, H. Tsujii, *Journal of Clinical Oncology* **25** (2007).

30. J. C. Williamson, J. Cao, H. Ihee, H. Frey, A. H. Zewail, *Nature* **386**, 159 (1997).

31. J. Yang, *et al.*, *Science* **368**, 885 (2020).

32. M. Lara-Astiaso, *et al.*, *The Journal of Physical Chemistry Letters* **9**, 4570 (2018).

33. J. Rak, P. Skurski, M. Gutowski, *The Journal of Chemical Physics* **114**, 10673 (2001).

34. NIST Atomic Spectra Database, Available: https://physics.nist.gov/asd National Institute of Standards and Technology, Gaithersburg, MD. (2018).

35. H. Bachau, P. Galan, F. Martín, A. Riera, M. Yáñez, *Atomic Data and Nuclear Data Tables* **44**, 305 (1990).

36. M. Karplus, R. H. Porter, *Atoms and molecules an introduction for students of physical chemistry* (New York W. A. Benjamin, 1970).

37. A. Macías, A. Riera, *Physics Reports* **90**, 299 (1982).

38. M. Barat, W. Lichten, *Phys. Rev. A* **6**, 211 (1972).

39. D. Vernhet, *et al.*, *Nuclear Instruments and Methods in Physics Research Section B: Beam Interactions with Materials and Atoms* **107**, 71 (1996).

40. J. Tabet, *et al.*, *Phys. Rev. A* **82**, 022703 (2010).

41. T. Jahnke, *et al.*, *Chemical Reviews* **120**, 11295 (2020).

42. M. Barat, P. Roncin, *Journal of Physics B: Atomic, Molecular and Optical Physics* **25**, 2205 (1992).

43. J. Eland, *Molecular Physics* **61**, 725 (1987).

44. J. H. D. Eland, *Laser Chemistry* **11**, 259 (1991).

45. R. Flammini, M. Satta, E. Fainelli, L. Avaldi, *Phys. Rev. A* **83**, 014501 (2011).

46. V. Bernigaud, *et al.*, *Publications de l'Observatoire Astronomique de Beograd* **84**, 83 (2008).

47. T. Bergen, *et al.*, *Rev. Sci. Instrum.* **70**, 3244 (1999).

48. F. Chandezon, B. A. Huber, C. Ristori, *Rev. Sci. Instrum.* **65**, 3344 (1994).

49. M. Capron, *et al.*, *Chem.-Eur. J.* **18**, 9321 (2012).

50. S. Maclot, *et al.*, *Phys. Rev. Lett.* **117**, 073201 (2016).

51. D. M. Curtis, J. H. D. Eland, *International Journal of Mass Spectrometry and Ion Processes* **63**, 241 (1985).

52. K. Schäfer, W. Y. Baek, K. Förster, D. Gassen, W. Neuwirth, *Zeitschrift fr Physik D Atoms, Molecules and Clusters* **21**, 137 (1991).

53. S. Tomita, H. Lebius, A. Brenac, F. Chandezon, B. A. Huber, *Phys. Rev. A* **65**, 053201 (2002).

54. T. H. Dunning Jr., *J. Chem. Phys.* **90**, 1007 (1989).

55. T. Shiozaki, *WIREs Comput Mol Sci* p. e1331 (2017).

56. I. Fernández Galván, *et al.*, *J. Chem. Theory Comput.* (2019).

57. M. Richter, P. Marquetand, J. González-Vázquez, I. Sola, L. González, *J. Chem. Theory Comput.* **7**, 1253 (2011).

58. J. W. Park, R. Al-Saadon, N. E. Strand, T. Shiozaki, *J. Chem. Theory Comput.* **15**, 4088 (2019).

Supplementary Information: Timing of charge migration in betaine by impact of fast atomic ions

P. Rousseau,[1,*] J. González-Vázquez,[2,3,*] D.G. Piekarski,[2,†] J. Kopyra,[4] A. Domaracka,[1] M. Alcamí,[2,3,5] L. Adoui,[1] B. A. Huber,[1] S. Díaz-Tendero,[2,3,6,‡] and F. Martín[2,5,6,§]

[1]*Normandie Univ, ENSICAEN, UNICAEN, CEA, CNRS, CIMAP, 14000 Caen, France.*

[2]*Departamento de Química, Módulo 13, Universidad Autónoma de Madrid, 28049 Madrid, Spain.*

[3]*Institute for Advanced Research in Chemical Sciences (IAdChem), Universidad Autónoma de Madrid, 28049 Madrid, Spain.*

[4]*Faculty of Exact and Natural Sciences, Siedlce University of Natural Sciences and Humanities, 3 Maja 54, 08-110 Siedlce, Poland.*

[5]*Instituto Madrileño de Estudios Avanzados en Nanociencias (IMDEA Nano), Cantoblanco 28049 Madrid, Spain*

[6]*Condensed Matter Physics Center (IFIMAC), Universidad Autónoma de Madrid, 28049 Madrid, Spain.*

(Dated: July 9, 2021)

* These authors contributed equally

† Present address: Institute of Physical Chemistry, Polish Academy of Sciences, Kasprzaka 44/52, 01-224 Warsaw, Poland.

‡ sergio.diaztendero@uam.es

§ fernando.martin@uam.es

S1. FULL ION-ION COINCIDENCE MAP

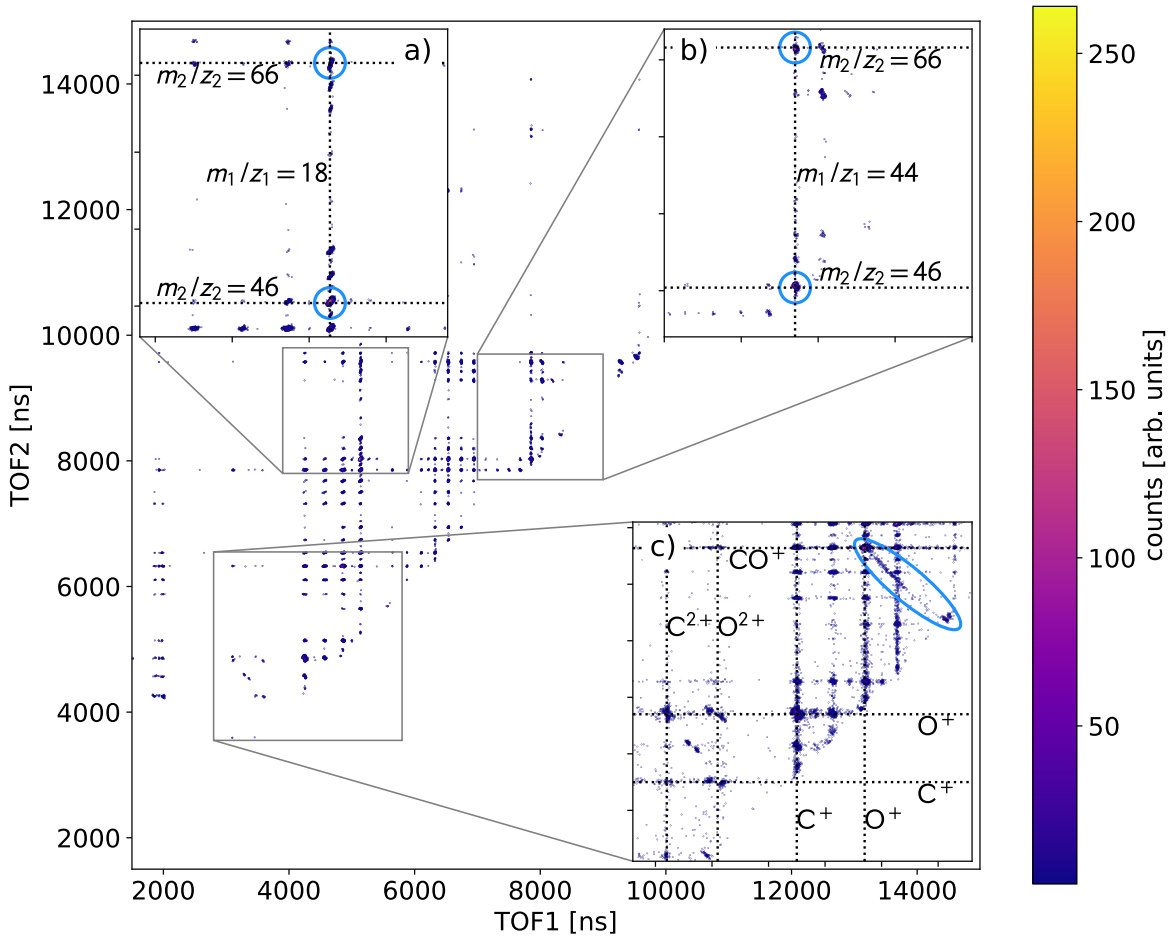

FIG. S1: **Full ion-ion coincidence map.** Full ion-ion coincidence map resulting from the fragmentation of fully deuterated betaine by impact of 3 keV/amu O^{6+}.

S2. EXTRACTION OF THE FRAGMENTS' KINETIC ENERGIES

In our experiment, the neutral betaine molecules are isotropically distributed in space. However, as explained in the main text, in the present case, double electron capture resulting from the collision can only occur for molecules whose negatively charged side faces the projectile. Hence, the probability to form a betaine dication will be maximum when the negatively charged side of neutral betaine (-CO_2) is in front of the projectile and zero when it is in the opposite side. Therefore, after the collision, the spatial distribution of doubly charged betaine molecules will be strongly anisotropic along the direction that connects the center of mass of the molecule with the projectile (see Fig. S2). The shape of the spatial distribution of doubly charged betaine molecules is the same for all projectile positions contained in a circle centered on the molecule with radius equal to the effective impact parameter in the collision (see Fig. S2). All these positions are equally accessible in the collision. To reflect the fact that the CO_2 side faces the projectile, the maximum of the probability distribution must always lie in the line connecting the center of the circle with the projectile position. In other words, the probability distribution must rotate in the YZ plane following the different positions of the projectile in the dashed green circle in Fig. S2. Therefore, the overall orientation of the doubly charged ions is nearly isotropic in the YZ plane. This plane contains the extraction direction. The same reasoning applies for projectiles not impinging perpendicularly to the plane shown in the figure.

Fig. S3 shows collision geometries in which a fragment is emitted in different directions relative to the extraction field for two different values of the momentum in each direction (represented by red and blue arrows). We have only considered those orientations that can lead to double charge transfer to the projectile, i.e., we are not considering orientations in which the negatively charge side of the target is on the opposite side of the projectile. We have considered the extreme cases where the momentum of the ejected fragment is parallel, perpendicular and antiparallel to the extraction field of the TOF mass spectrometer (along the Z-axis) and two intermediate cases. The parallel and antiparallel cases correspond to, respectively, the shortest and longest time of flights of the charged fragment. In these cases, the total momentum of the fragment is entirely given by the Z-component (the X- and Y-components are close to zero), so that we can determine the total kinetic energy of the fragment. All other cases result in time of flights that lie in between these two extremes.

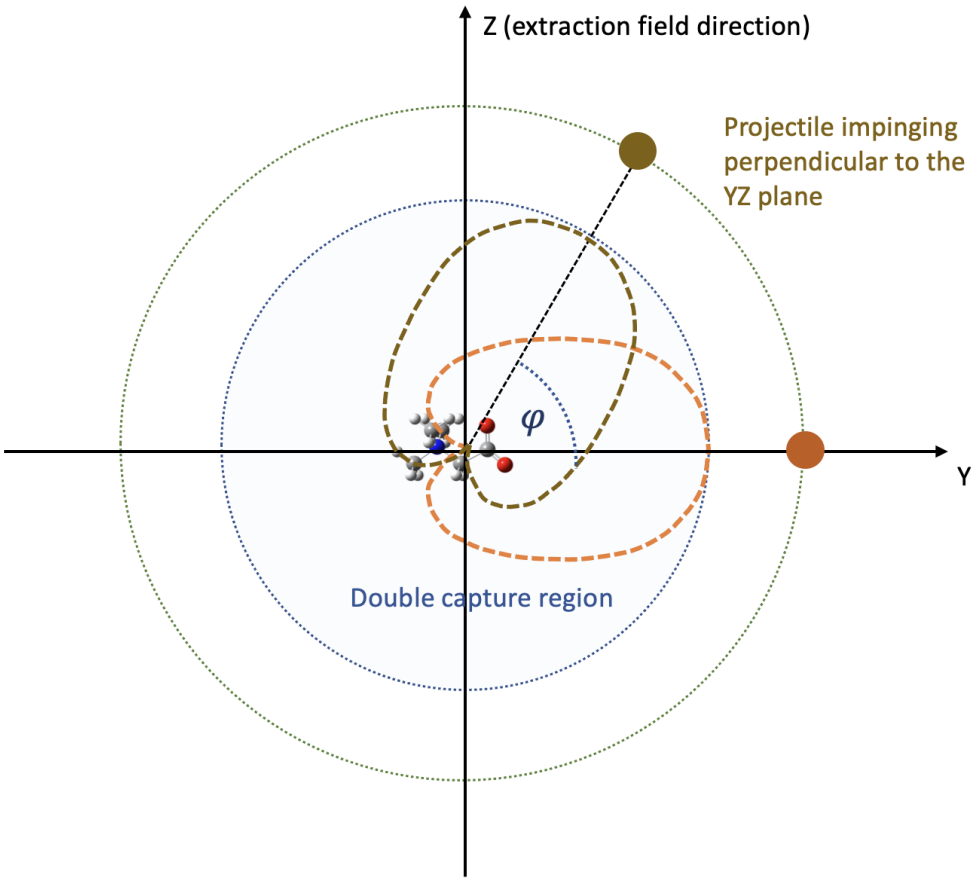

FIG. S2: **The collision geometry.** Estimated double capture probability (dashed thick lines) for ions (full circles) impinging perpendicular to the the YZ plane as a function of the angle ϕ between the line connecting the center of mass of the molecule and the projectile. Notice that the probability is maximum when the projectile is just in front of the negatively charged side of betaine and is zero when it is in the opposite side (see main text). This probability distribution rotates following the different positions of the projectile in the dashed green circle. Therefore, the overall orientation of the doubly charged ions is isotropic in the YZ plane. The same reasoning applies for projectiles not impinging perpendicularly to the YZ plane.

As the distribution of molecular dications that can lead to this specific fragment is isotropic in the plane containing the direction of the extraction field (see above), for a given kinetic energy of a fragment one expects a flat time-of-flight distribution connecting the shortest and longest time of flights (red and blue rectangular distributions in the figure). The width of this distribution depends on the kinetic energy of the fragment (as shown by the red and

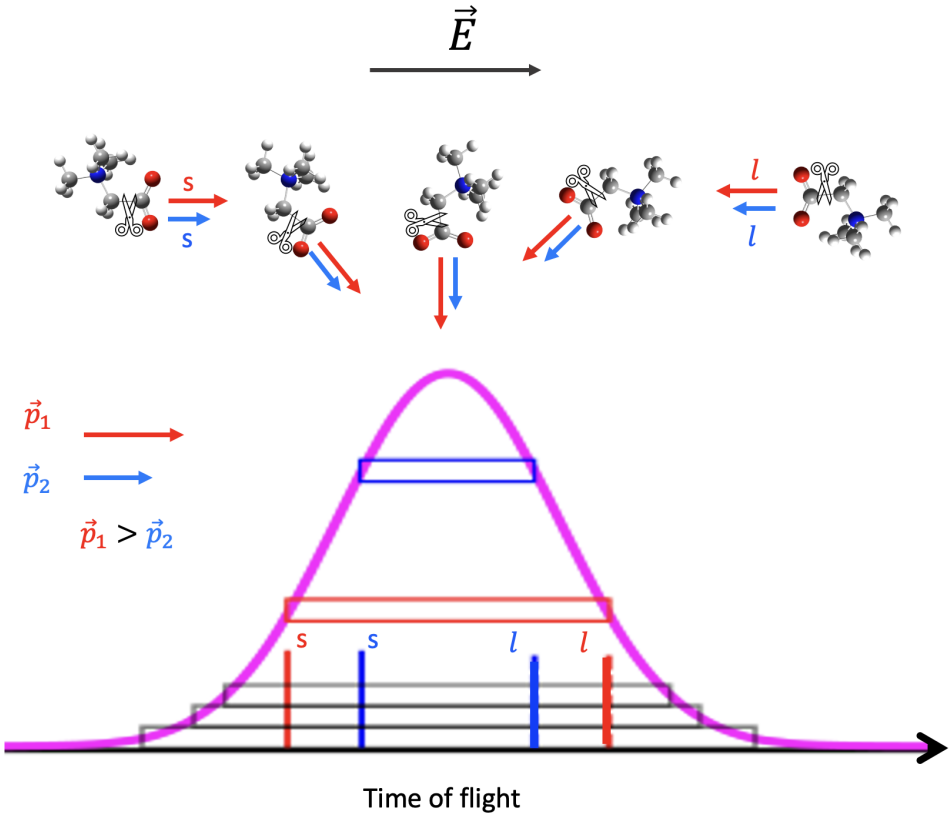

FIG. S3: **Connection between the measured TOF signal and the kinetic energy of the fragments.** As an illustration, CO_2^+ emission from five different molecular orientations in the plane perpendicular to the projectile incidence direction are considered. The field (E) extraction direction is indicated by a black arrow. Two different values of the fragment momentum are considered (red and blue arrows). The parallel and antiparallel cases correspond to the shortest (s) and longest (l) time of flights of the charged fragment. All intermediate cases lead to time of flights in between these extreme values. The width of the TOF distribution depends on the kinetic energy of the fragment (as shown by the red and blue rectangular distributions) and, therefore, it is directly related to the kinetic energy of that fragment. The stacking of rectangular distributions for each value of the kinetic energy leads to the observed TOF distribution.

blue rectangular distributions) and, therefore, it is directly related to the kinetic energy of that fragment. The TOF peak is thus made by the stacking of rectangular distributions with different widths (thus different kinetic energies, see black rectangles). In this way the KE distribution can be obtained by simply analyzing the shape of the TOF-peak or the

KER distribution by the shape of the TOF2-TOF1 peak obtained from the coincidence ion pair. During the treatment of the data some resolution is lost compared to a full momentum measurement with position sensitive detectors, but it is enough for the purpose of understanding the mechanisms described in the manuscript.

Noteworthy, in the present TOF spectrometer, the transmission efficiency of the fragment is close to 100% up to kinetic energies of about 10 eV. Moreover, the Daly-type detector also gives high and uniform detection efficiency over a large mass range (the TOF system was designed for the study of metallic clusters and successfully used for clusters of C_{60} molecules). The observation of well-defined slopes also shows that the coincidences are not fortuitous and that the probability to miss one fragment in the case of 3 charged fragments events is low enough to avoid a significant contribution of these events in the recorded 2-stops events. For instance, in the case of the island 18+/66+, it is clear that the third fragment is neutral (and with a significant momentum) and not a charged one that was not detected.

S4. EXTENDED MOLECULAR DYNAMICS CALCULATIONS

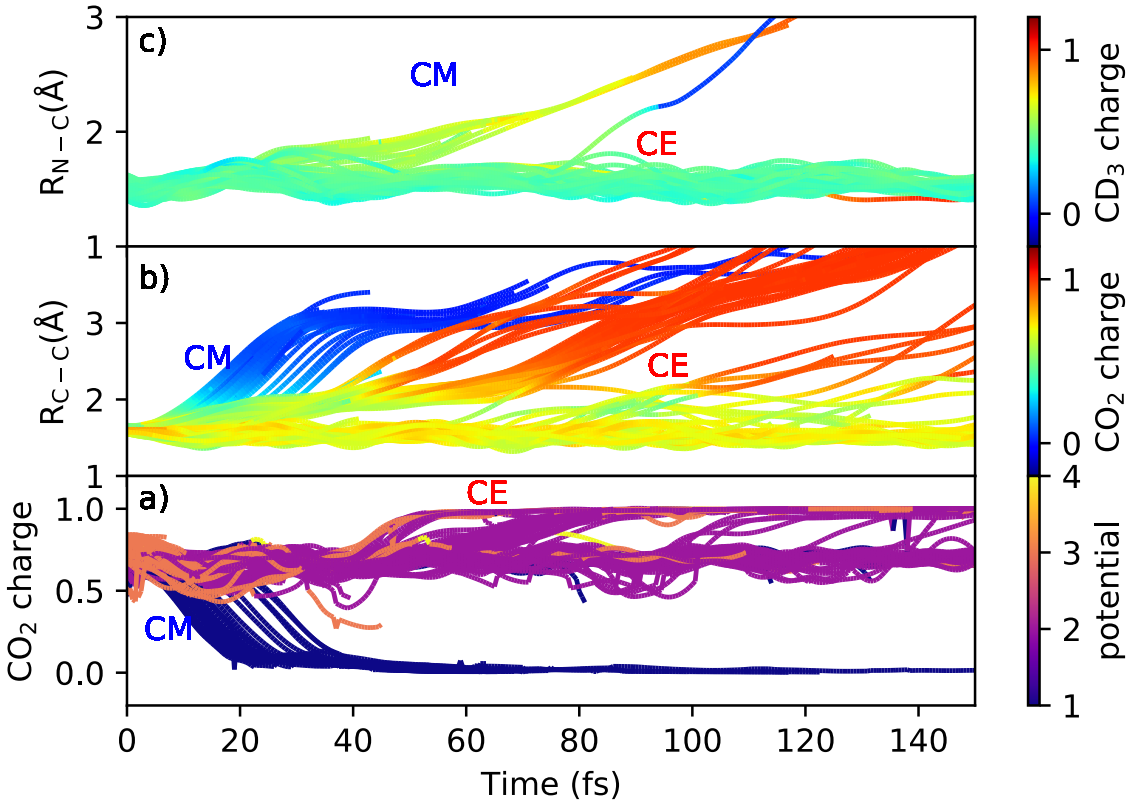

FIG. S4: **Extended molecular dynamics calculations.** Molecular dynamics calculations extended up to 150 fs. (a) Evolution of the charge located at the CO_2 end of doubly-charged betaine for all trajectories starting in the ground (1), the first (2) and the second (3) excited state. The color palette on the right indicates the potential energy surface in which the trajectory evolves at every time. (b) Evolution of the $C_{carboxylate}-C_{\alpha}$ bond distance. The color palette on the right indicates the charge in the CO_2 end at every time. (c) Evolution of the C_N-C bond distance. The color palette on the right indicates the charge in the CD_3 site at every time.

S5. ADIABATICITY OF CHARGE MIGRATION

We have performed XMS-CASPT2 calculations to obtain the electronic states of doubly charged betaine along the minimum energy path (MEP) that leads to emission of neutral CO_2 in the ground electronic state (the charge migration channel). We have also calculated the overlap between ground state wave functions in consecutive points of the MEP in order to visualize possible changes of electronic character along the MEP. The results are shown in Fig. S5.

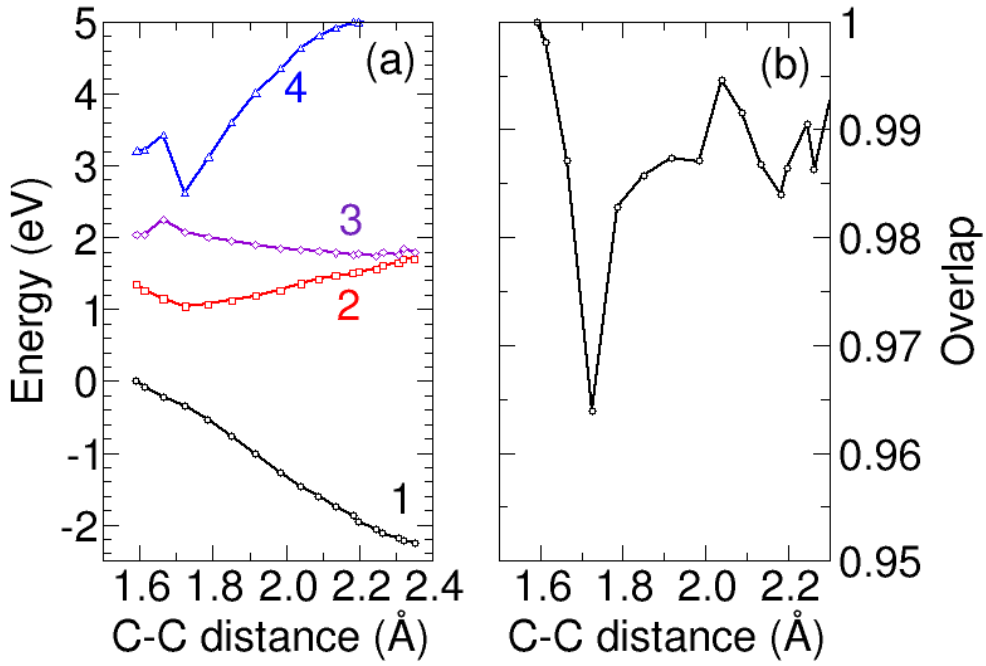

FIG. S5: **Adiabaticity of charge migration.** (a) Electronic energies of the betaine dication (XMS-CASPT2 level) along the minimum energy path (MEP) leading to CO_2 emission in the ground electronic state. Black line: ground state; red line: first excited state; purple line: second excited state; blue line: third excited state. (b) Overlap between electronic ground states obtained in consecutive points of the MEP.

As can be seen, along the whole MEP, the energy separation between the ground and the lowest excited state of the betaine dication is never less than 1 eV and this energy separation increases as the CO_2 fragment departs from the molecular dication. Thus, we can conclude that no sharp curve crossing is contributing to the production of neutral CO_2. We can also

discard a change of character in the ground state electronic wave function, since the overlap between ground state wave functions in consecutive points of the MEP is always above 0.96, indicating that the electronic character of the ground state remains roughly the same along the MEP. Therefore, the production of neutral CO_2, hence charge migration, is mainly an adiabatic process.